Energy & Environmental Science

PAPER

View Article Online
View Journal

Cite this: DOI: 10.1039/c8ee01270a

Hierarchical CoP/Ni_5P_4/CoP microsheet arrays as a robust pH-universal electrocatalyst for efficient hydrogen generation†

Ishwar Kumar Mishra,‡[a] Haiqing Zhou,‡[ab] Jingying Sun,[a] Fan Qin,[c] Keshab Dahal,[a] Jiming Bao,[c] Shuo Chen *[a] and Zhifeng Ren *[a]

Highly active catalysts composed of earth-abundant materials, performing as efficiently as Pt catalysts, are crucial for sustainable hydrogen production through water splitting. However, most efficient catalysts consist of nanostructures made *via* complex synthetic methods, making scale-up quite challenging. Here we report an effective strategy for developing a very active and durable pH-universal electrocatalyst for the hydrogen evolution reaction (HER). This catalyst is constructed using a sandwich-like structure, where hierarchical cobalt phosphide (CoP) nanoparticles serve as thin skins covering both sides of nickel phosphide (Ni_5P_4) nanosheet arrays, forming self-supported sandwich-like CoP/Ni_5P_4/CoP microsheet arrays with lots of mesopores and macropores. The as-prepared electrocatalyst requires an overpotential of only 33 mV to achieve a benchmark of 10 mA cm^{-2}, with a very large exchange current density and high turnover frequencies (TOFs) in acid media, superior to most electrocatalysts made of metal phosphides, well-known MoS_2 and WS_2 catalysts, and it performs comparably to state-of-the-art Pt catalysts. In particular, this electrocatalyst shows impressive operational stability at an extremely large current density of 1 A cm^{-2}, indicating its possible application toward large-scale water electrolysis. Additionally, this electrocatalyst is very active in alkaline electrolyte (71 mV at 10 mA cm^{-2}), which demonstrates its pH universality as a HER catalyst with outstanding catalytic activity. This simple strategy does not involve any solvothermal and hydrothermal processes, paving a new avenue toward the design of robust non-noble electrocatalysts for hydrogen production, aimed at commercial water electrolysis.

Received 1st May 2018,
Accepted 25th May 2018

DOI: 10.1039/c8ee01270a

rsc.li/ees

Broader context

Hydrogen is an ideal energy carrier for replacing carbon-containing fuels due to its high energy density and zero pollution gas emission. Water electrolysis is very appealing for producing hydrogen on a large scale, with the benefits of low cost, high purity and renewability, but it requires robust and stable electrocatalysts to expedite the reaction kinetics. On earth, there are various water sources including acidic, alkaline, and industrial waste water, and seawater with different pH values, which could possibly be used for hydrogen production. In fact, there are many water electrolysis technologies with different demands on the pH values of the electrolytes, including proton exchange membrane electrolysis in strong acids, microbial electrolysis and sea-water electrolysis in neutral solutions, and commercially used water electrolysis in bases. Thus, developing efficient and cheap electrocatalysts operating well over a wide solution-pH range for hydrogen evolution is highly desirable. Here we introduce an effective approach for developing an active and durable pH-universal electrocatalyst, constructed with CoP/Ni_5P_4/CoP microsheet arrays forming a sandwich-like structure. This electrocatalyst is very active for hydrogen evolution in strong acids and bases, showing good durability at large current densities. This discovery paves a new avenue toward the rational design of robust non-noble metal-containing electrocatalysts for water splitting.

[a] *Department of Physics and TcSUH, University of Houston, Houston, TX 77204, USA. E-mail: schen34@uh.edu, zren@uh.edu*
[b] *Key Laboratory of Low-Dimensional Quantum Structures and Quantum Control of Ministry of Education, School of Physics and Electronics, Hunan Normal University, Changsha 410081, China*
[c] *Department of Electrical and Computer Engineering, University of Houston, Houston, TX 77204, USA*

† Electronic supplementary information (ESI) available: Experimental details and results. See DOI: 10.1039/c8ee01270a

‡ These authors contributed equally to this work.

Hydrogen produced *via* water electrolysis is a clean energy carrier, which can be regarded as a potential alternative to fossil fuels.[1–4] Water dissociation for hydrogen production *via* electrolysis requires highly active catalysts to minimize overpotentials. Platinum (Pt)-based materials are the most active electrocatalysts for the hydrogen evolution reaction (HER). However, noble-metal based catalysts are not suitable for large-scale application due to their high cost and the limited availability of noble-metals in the earth's crust.[5,6] For a sustainable and

clean hydrogen economy, highly active and affordable catalysts based on earth-abundant materials have to be developed.

Noble metal-free materials, including metal sulfides, selenides, phosphides, *etc.*, have been widely explored for catalyzing the HER.[7–10] Among these, transition-metal phosphides (TMPs) have received significant attention due to their promising catalytic activity toward the HER in water splitting.[11,12] In past years, several efficient TMP-based materials have been explored for the HER, including Ni_2P,[10] Mo–W–P,[13] CoP/CC,[14] CoPS,[15] and $Fe_xCo_{1-x}P$.[16] Despite considerable achievements, it still remains a large challenge to design and develop catalysts consisting of earth-abundant materials with Pt-like pH-universal HER activity and promising operational stability at high current densities (>500 mA cm^{-2}), considering the poor long-term stability of Pt catalysts in both acidic and alkaline media.[17] Indeed, little attention has been given to structural design to enhance catalytic activity and long-term durability, especially at even higher current densities (>2 A cm^{-2}), which is crucial for large-scale hydrogen production through electrocatalytic water splitting. In particular, many catalysts require complicated preparation procedures, which are not industrially compatible. What's more, an ideal electrocatalyst is expected to exhibit outstanding catalytic HER activity over a wide pH range (0–14) similarly to Pt, considering the abundant sources of water on earth, and the different water electrolysis technologies with different demands on the pH values of electrolytes.[14,18,19] However, very few non-noble metal electrocatalysts are simultaneously robust in catalyzing the HER in both acidic and alkaline media. Thus, developing robust catalysts with pH universality and long-term durability at high current densities remains challenging. In this work, we report the rational design of a highly active electrocatalyst based on a sandwich-like hybrid of cobalt and nickel phosphides for the HER in water splitting. Cobalt phosphide (CoP) nanoparticles were designed to cover nickel phosphide (Ni_5P_4) nanosheet arrays, forming self-supported microsheet arrays. Benefiting from the sandwich-like design of the active material, a hierarchical CoP/Ni_5P_4/CoP microsheet array electrode shows Pt-like activity toward the HER, with pH universality and exceptional stability. In 0.5 M H_2SO_4, it requires overpotentials of only 33 and 85 mV to achieve current densities of 10 and 100 mA cm^{-2}, respectively, with a relatively small Tafel slope of 43 mV dec^{-1} and a large exchange current density of 1.708 mA cm^{-2}, and it exhibits a large surface area and simultaneously high turnover frequencies (TOF) of 0.453 and 1.22 H_2 s^{-1} at 75 and 100 mV overpotentials, respectively, outperforming most efficient non-noble-metal HER electrocatalysts that have been reported so far. In particular, this robust catalyst shows excellent durability at a high current density of 1 A cm^{-2}. Moreover, the as-prepared CoP/Ni_5P_4/CoP microsheet array electrode only requires 71 mV to deliver 10 mA cm^{-2} in 1 M KOH, and also exhibits good durability at 30 and 500 mA cm^{-2}, demonstrating its pH universality for efficient hydrogen production.

The synthesis of the CoP catalyst involves a three-step process, as illustrated in Fig. 1. First, nickel (Ni) foam was thermally phosphorized at 500 °C in a tube furnace using red phosphorous (P) to form nickel phosphide nanosheet arrays,[20]

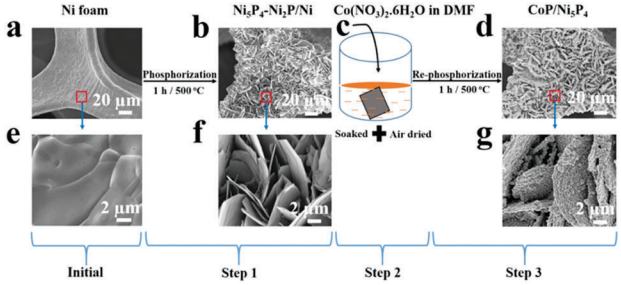

Fig. 1 Synthetic scheme for the sandwich-like CoP/Ni_5P_4/CoP electrocatalyst. (a and e) SEM images of the Ni foam used as the starting electrode material. (b and f) SEM images of the nickel phosphide nanosheet arrays after the first synthetic step. (c) A diagram showing the nickel phosphide nanosheets on Ni foam that were soaked in a cobalt precursor ink prepared by dissolving cobalt nitrate hexahydrate [$Co(NO_3)_2{\cdot}6H_2O$] in DMF. (d and g) SEM images of the hierarchical CoP/Ni_5P_4/CoP microsheet arrays after the third synthetic step.

as demonstrated in the scanning electron microscopy (SEM) images in Fig. 1b and f. Second, the nickel phosphide nanosheet arrays on Ni foam were soaked in Co-ink and dried under ambient conditions (Fig. 1c). The cobalt (Co) precursor ink was prepared by dissolving cobalt nitrate hexahydrate [$Co(NO_3)_2{\cdot}6H_2O$] in *N*,*N*-dimethylformamide (DMF). The firmly constructed structure (Fig. 1b and f) as well as the hydrophilic nature of the nickel phosphide nanosheets facilitated the development of uniform coverage of the nanosheets by the Co precursor ink. Finally, a dried sample was thermally phosphorized again at 500 °C, leading to the formation of a uniquely structured hierarchical CoP/Ni_5P_4/CoP microsheet array electrode, as revealed in the SEM images in Fig. 1d and g.

The surface morphology of the CoP/Ni_5P_4/CoP microsheet array electrode changes greatly upon varying the concentration of precursor Co-ink (Fig. S1, ESI†). With a precursor ink concentration of 0.25 g ml^{-1}, most of the nickel phosphide nanosheets were uniformly covered by CoP after phosphorization (Fig. S1b and e, ESI†), leading to the extremely large surface exposure of cobalt phosphide, and the formation of a sandwich-like structure between CoP nanoparticles and Ni_5P_4 nanosheets, as confirmed by an SEM image (Fig. S2, ESI†). When the concentration was increased to 0.4 g ml^{-1}, all the interspaces between the nanosheets were filled with the cobalt precursor, and the nickel phosphide nanosheets were buried (Fig. S1a and d, ESI†), thereby reducing the exposed surface of CoP. On the other hand, at a very low concentration of precursor ink (0.1 g ml^{-1}), most of the nickel phosphide nanosheets were not covered with CoP (Fig. S1c and f, ESI†). Since the optimum coverage of nickel phosphide nanosheets was achieved at a Co precursor ink concentration of 0.25 g ml^{-1}, further analyses were carried out using this concentration, unless otherwise mentioned. Meanwhile, in order to examine the role of phosphorus, a sample was also prepared by annealing in the absence of a phosphorus source during the third step, for comparison. A notably different morphology was observed in the absence of a phosphorus source (Fig. S3a and b, ESI†), which may be due to the formation of a different cobalt chemical compound.

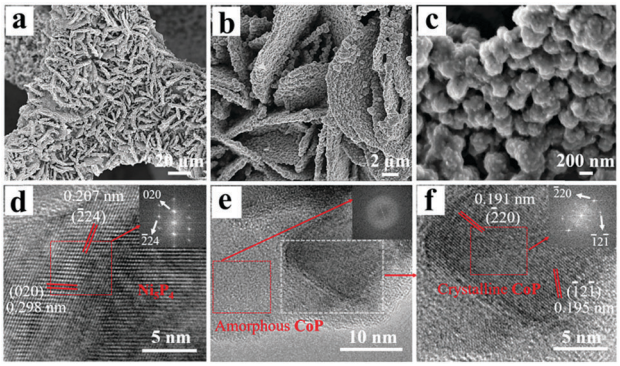

Fig. 2 The morphology and chemical composition of the CoP/Ni_5P_4/CoP electrocatalyst. (a–c) Typical SEM images of the CoP/Ni_5P_4/CoP electrode. (d) A HRTEM image showing crystalline Ni_5P_4 in the inner structure of the CoP/Ni_5P_4/CoP electrode. The fast Fourier transform (FFT) in the inset demonstrates the crystal structure of Ni_5P_4. (e and f) HRTEM images showing amorphous as well as crystalline CoP in the outer structure of the CoP/Ni_5P_4/CoP electrode. The FFTs in the insets of (e) and (f) demonstrate the amorphous and crystalline structures of CoP, respectively.

In addition, morphology variations with temperature were also investigated through phosphorization at 600 °C during the third synthesis step. At 600 °C, a prominent change in the surface structure of CoP was observed in SEM images, as seen in Fig. S4 (ESI†), which is due to structural deformation of the inner frame of the nickel phosphide nanosheets as well as the outer cobalt phosphide coverage at a higher temperature.

The high resolution SEM images in Fig. 2a–c display a closer view of the surface morphology of CoP, demonstrating the porous structure of the interconnected nanostructures, composed of macropores from the Ni foam and nickel phosphide nanosheets and mesopores from the CoP particles (Fig. S5 and S6, ESI†), which may contribute to the excellent HER catalytic activity by facilitating the exposure of numerous active sites, and also offering efficient diffusion channels during H_2 evolution in water splitting. In order to gain further insight into the crystalline structure, the as-prepared electrocatalyst was examined *via* transmission electron microscopy (TEM) (Fig. 2d–f). The high-resolution transmission electron microscopy (HRTEM) image in Fig. 2d clearly demonstrates that the nickel phosphide nanosheets are highly crystallized with lattice fringe spacings of 0.207 nm and 0.298 nm, corresponding to the (2̄24) and (020) planes of Ni_5P_4 crystals, respectively. Accordingly, the outer coverage of the electrode indicates a mixed structure, showing that a small fraction crystallizes corresponding to the (2̄20) and (12̄1̄) planes of CoP crystals, along with amorphous CoP being present, as revealed in the HRTEM images in Fig. 2e and f. Furthermore, X-ray energy dispersive spectroscopy (EDS) elemental mapping confirms the uniform distribution of Co and P along with a small fraction of Ni, with an atomic ratio of Co : P of 1 : 0.93, which is very close to the 1 : 1 ratio of CoP, indicating the formation of CoP in the as-prepared electrode (Fig. S7, ESI†). The small fraction of Ni in the EDS mapping could be either from Ni_5P_4 that remained while peeling off the cobalt phosphide from the electrode during TEM sample preparation or from the diffusion of Ni from the inner support during synthesis.

Powder X-ray diffraction (XRD) was employed to further characterize the phase compositions of the samples and to determine the rough atomic ratio of different elements. Typical XRD patterns from the as-prepared nanosheet arrays after step 1 demonstrate a mixture of nickel phosphides, mainly Ni_5P_4, with a minor amount of Ni_2P and a small amount of metallic Ni (Fig. 3a), suggesting that the original Ni foam was not fully transformed to nickel phosphide. Interestingly, the XRD pattern of an electrode prepared with re-phosphorization after step 3 shows mostly Ni_5P_4, along with a small shoulder at a 2-theta position of around 48°, corresponding to a CoP phase. The disappearance of Ni_2P and Ni after re-phosphorization may result from the diffusion of the P source into the nickel and nickel phosphide, converting them to a Ni_5P_4 phase. To support this statement, we carried out a second phosphorization of nickel phosphide nanosheet samples under the same conditions as those for CoP growth. The XRD pattern (Fig. S8, ESI†) is the same as that of Ni_5P_4 crystals, confirming the conversion of the mixed Ni_5P_4/Ni_2P/Ni phase to a high-purity Ni_5P_4 phase during CoP growth. On the other hand, the small CoP peak in the XRD patterns indicates the presence of only a small fraction of CoP crystals; the rest could be amorphous CoP or this could simply be because of the very thin thickness of CoP on top of Ni_5P_4, further supporting the mixed composition of CoP in the as-prepared hierarchical CoP/Ni_5P_4/CoP electrode, as revealed in HRTEM images. In addition, compared to the nickel phosphide in the inner support structure, a similar phase

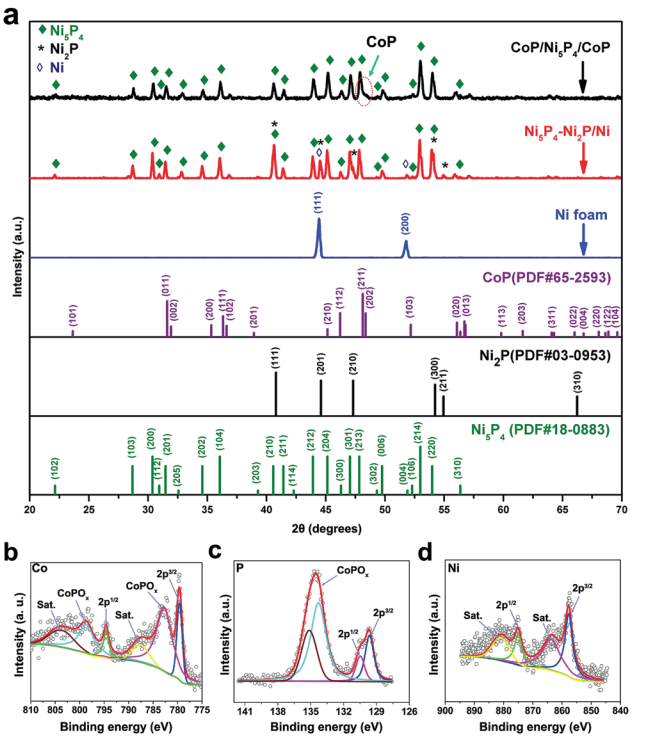

Fig. 3 Characterization of the CoP/Ni_5P_4/CoP microsheet array electrode. (a) Typical XRD patterns showing the phase structure of Ni foam, the Ni_5P_4–Ni_2P/Ni support and the CoP/Ni_5P_4/CoP electrode. Detailed XPS analysis of: (b) Co 2p; (c) P 2p; and (d) Ni 2p spectra.

composition was noticed in a sample prepared *via* annealing only during the third synthetic step (Fig. S9, ESI†), which indicates no further phase change in the nickel rich phosphides in the absence of an additional P source. Moreover, the absence of a shoulder in the XRD patterns at a 2-theta angular position of around 48° for the sample prepared with annealing only further supports the idea that the small shoulder from the sample prepared *via* re-phosphorization during the third synthetic step is from CoP crystals.

X-ray photoelectron spectroscopy (XPS) was utilized to study the surface chemical compositions of the samples. According to high-resolution XPS spectra of the hierarchical CoP/Ni_5P_4/CoP array electrode, we can easily identify the presence of Co, P, and Ni (Fig. 3b–d and Fig. S10, Table S1, ESI†). The Co core level peaks (Fig. 3b) appear at binding energies (BEs) of 779.6 eV and 794.6 eV, corresponding to Co $2p^{3/2}$ and $2p^{1/2}$ of cobalt phosphide,[14] respectively. In the XPS spectra of Co 2p, some contribution from an oxidized component of cobalt phosphide is also observed at BEs of 782.7 eV and 798.6 eV, corresponding to $2p^{3/2}$ and $2p^{1/2}$,[14] respectively. The P core level peaks (Fig. 3c) are located at 129.6 eV and 130.5 eV, which correspond to P $2p^{3/2}$ and $2p^{1/2}$ of CoP,[14,16] respectively. In the XPS spectra of P 2p, peaks at BEs of 134.3 eV and 135.1 eV correspond to the oxidized states $2p^{3/2}$ and $2p^{1/2}$, respectively, which originate from the surface oxidation of CoP.[13,14,20,21] In addition, Ni core level peaks (Fig. 3d) are also observed at BEs of 857.7 eV and 875.0 eV, which originate from Ni $2p^{3/2}$ and $2p^{1/2}$ of surface oxidized nickel phosphide,[22,23] respectively, which possibly arise from protruding nickel phosphide nanosheets (Fig. S11, ESI†). The protruding part possibly results from the formation of P-rich nickel phosphide (Ni_5P_4) phases from diffused P during re-phosphorization, and such a feature is observed only in a few regions of the electrode. Furthermore, the BE of Co 2p centered at 779.6 eV is positively shifted from the position of elemental Co (778.1–778.2 eV), and that of P 2p centered at 129.6 eV is negatively shifted from the position of elemental P (129.9 eV), which implies that Co carries a partial positive charge (δ^+) and P carries a partial negative charge (δ^-) in CoP.[14,24] The metal center Co (δ^+) and pendant base P (δ^-) in CoP resembles hydrogenases and other metal complex HER catalysts, indicating the similar catalytic mechanism of CoP with respect to these.[25,26]

The electrochemical HER performance of the as-prepared electrocatalyst was first assessed in 0.5 M H_2SO_4, and a scan rate of 2 mV s^{-1} was set to collect the polarization curves *via* linear sweep voltammetry in a three-electrode setup (Fig. S12, ESI†).[27] All the potentials used here were converted to values relative to a reversible hydrogen electrode (RHE). Fig. 4a presents the relevant polarization curves of different electrodes, including hierarchical CoP/Ni_5P_4/CoP microstructured arrays, pure Ni foam, Pt wire, and the Ni_5P_4–Ni_2P/Ni nanosheet array support. The CoP/Ni_5P_4/CoP electrocatalyst shows a fast increase in cathodic current density with increasing overpotential, suggesting that CoP/Ni_5P_4/CoP is a high-performance 3D cathode for hydrogen generation from water splitting. At a geometric current density of 10 mA cm^{-2}, the as-prepared hierarchical

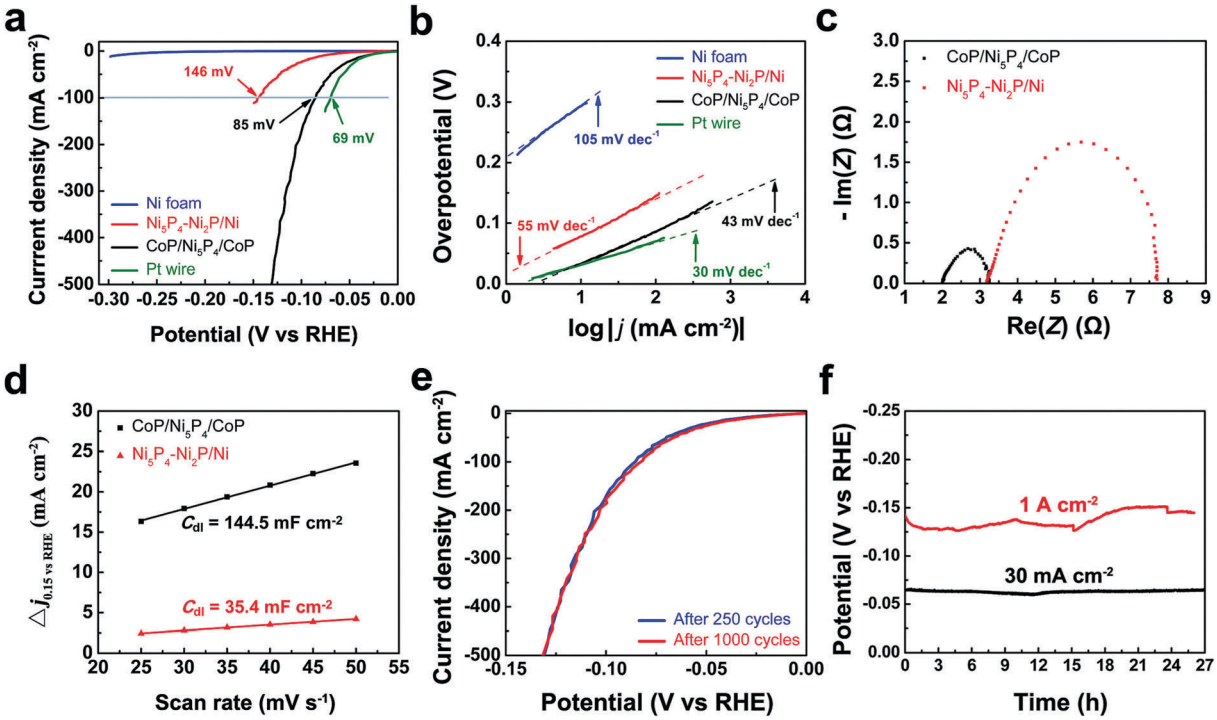

Fig. 4 Electrocatalytic measurements for different electrodes during hydrogen evolution in acid. (a) Polarization curves of CoP/Ni_5P_4/CoP, Ni_5P_4–Ni_2P/Ni, pure Ni foam, and Pt wire electrodes. (b) Tafel plots derived from the curves in (a). (c) EIS Nyquist plots of CoP/Ni_5P_4/CoP and Ni_5P_4–Ni_2P/Ni electrodes. (d) The double-layer capacitance (C_{dl}) of CoP/Ni_5P_4/CoP and Ni_5P_4–Ni_2P/Ni electrodes. (e) Polarization curves of the CoP/Ni_5P_4/CoP electrode after 250 and 1000 cycles. (f) Testing the potential of the CoP/Ni_5P_4/CoP electrode at constant current densities of 30 mA cm^{-2} and 1 A cm^{-2}.

CoP/Ni_5P_4/CoP 3D electrode requires an overpotential of only 33 mV, which is very close to that of Pt (31 mV), and much lower than the 293 mV required by pure Ni foam and the 79 mV required by the Ni_5P_4–Ni_2P/Ni support. Compared to the samples prepared with 0.4 and 0.1 g ml^{-1} concentrations of precursor Co-ink during the second synthetic step, the sample prepared with 0.25 g ml^{-1} exhibits much better electrocatalytic performance (Fig. S13, ESI†), which is possibly due to the greater exposure of active surfaces, as revealed in the SEM images in Fig. S1b and e (ESI†). In contrast, the catalytic activity of the sample prepared by annealing only during step 3 of the synthesis shows poorer HER performance (Fig. S14, ESI†), similar to the Ni_5P_4–NiP_2/Ni support, which is possibly due to the formation of cobalt oxide rather than cobalt phosphide in the absence of a P source. This oxide is not stable during water electrolysis, as supported by SEM images taken after electrochemical testing (Fig. S3c, ESI†), which shows that the outer layer of the cobalt compound was washed away by the highly corrosive acidic electrolyte during electrochemical potential cycling, leaving behind the nickel phosphide nanosheet array skeleton.

On the other hand, the phosphorization temperature during step 3 of the synthesis plays an important role in the morphology of the hierarchical CoP/Ni_5P_4/CoP, which accordingly has a great effect on the electrocatalytic HER activity; it is confirmed that 500 °C is the optimal temperature for growing this sandwich-like CoP/Ni_5P_4/CoP electrocatalyst (Fig. S15, ESI†). In particular, the electrocatalytic performance of CoP/Ni_5P_4/CoP grown at 500 °C is much better than those of many other highly efficient HER electrocatalysts reported recently (Table S2, ESI†), including nanostructured Ni_2P (105 mV),[10] Mo–W–P/carbon cloth (100 mV),[13] $WS_{2(1-x)}Se_{2x}$/$NiSe_2$ (88 mV),[28] $MoS_{2(1-x)}Se_{2x}$/$NiSe_2$ (69 mV),[29] CoP/carbon cloth (67 mV),[14] Ni/Ni_5P_4/NiP_2 (61 mV),[18] CoNiP (60 mV),[30] CoPS (48 mV),[15] $Fe_{0.5}Co_{0.5}P$ (37 mV),[16] *etc.* In addition, a Tafel slope of 43 mV dec^{-1} (Fig. 4b), derived from the polarization curve, indicates that the HER process using this CoP/Ni_5P_4/CoP electrode proceeds through a Volmer–Heyrovský mechanism.[31] Moreover, from the relevant Tafel plot, we can calculate the exchange current density to be 1.708 mA cm^{-2} for the CoP/Ni_5P_4/CoP catalyst (Table S2, ESI†), which is significantly larger than that for most of the reported active catalysts based on transition metal chalcogenides including $CoSe_2$,[9] and transition metal phosphides including WP_2 nanowire/CC,[32] CoP,[14] Ni_2P,[10] and MoP particles.[33] Finally, to further explore the superior catalytic performance of this sandwich-like catalyst, we quantified its TOF values at different overpotentials using a normal electrochemical method (Fig. S16, ESI†). This parameter is a very important performance index, representing the intrinsic catalytic activity of the catalyst. As shown in Table S3 (ESI†), the TOF values are evaluated to be around 0.453 and 1.220 H_2 s^{-1} at overpotentials of 75 and 100 mV, respectively. In particular, the TOF value increases to 4 H_2 s^{-1} at only 135 mV (Fig. S17, ESI†). Thus, this sandwich-like CoP/Ni_5P_4/CoP is found to have a very low overpotential (33 mV), a small Tafel slope (43 mV dec^{-1}), an extremely large exchange current density (1.708 mA cm^{-2}), and a very large TOF value of 4 H_2 s^{-1} at 135 mV, suggesting its exceptional H_2-evolving efficiency.

The physical origins of the electrode kinetics were further examined *via* electrochemical impedance spectroscopy (EIS) at a potential of −0.150 V *vs.* RHE, and the EIS Nyquist plots (Fig. 4c) can be well-fitted *via* a simplified Randles circuit (Fig. S18, ESI†). The series (R_s) and charge-transfer (R_{ct}) resistances are extracted from the fitted plots. Obviously, R_{ct} of the CoP/Ni_5P_4/CoP microsheet array electrode is 1.2 Ω, meaning very fast charge transfer occurs between the electrolyte and the catalyst. Also, there is a small R_s value (2.0 Ω) for this catalyst, which reflects the strong electrical integration of the catalyst with its support. To unveil the difference in intrinsic catalytic activity between the Ni_5P_4–Ni_2P/Ni support and CoP/Ni_5P_4/CoP microsheet array (Table S4, ESI†), we adopted a cyclic voltammetry (CV) method (Fig. 4d and Fig. S19, ESI†) to derive the electrochemical double-layer capacitance (C_{dl}),[20,29,34] which is directly related to the electrochemically active surface area (ECSA) of an electrocatalyst. Obviously, there is a large electrochemical surface area and roughness factor due to the presence of mesopores, nanosheet arrays and macropores in the catalyst (Table S3, ESI†). Then the exchange current density ($j_{0,normalized}$) is further normalized using the C_{dl} values, which is a useful parameter to compare intrinsic catalytic activity. After normalization (Table S4, ESI†), we find that the normalized exchange current density of this CoP/Ni_5P_4/CoP catalyst is 625.6 μA cm^{-2}, which is still far larger than that (366.1 μA cm^{-2}) of the Ni_5P_4–Ni_2P/Ni support, demonstrating that the CoP/Ni_5P_4/CoP catalyst has a higher intrinsic catalytic activity than a Ni_5P_4–Ni_2P/Ni nanosheet array-based catalyst. The exchange current density of the as-prepared CoP/Ni_5P_4/CoP catalyst compares favorably with most of the highly efficient electrocatalysts reported so far (Table S2, ESI†). Thus, according to C_{dl} measurements and EIS analysis, the CoP/Ni_5P_4/CoP electrode has much more favorable electrode kinetics toward hydrogen evolution, which could be related to the following factors: (1) the strong contact of CoP with the inner Ni_5P_4 support, which enables good mechanical and electrical connection, providing an easy pathway for electrons to flow during cathodic polarization; (2) the excellent electrical conductivity of CoP facilitating fast charge transport; and (3) the 3D structure along with the highly porous features of the interconnected nanostructures enabling greater exposure of active sites for hydrogen adsorption as well as easy diffusion pathways for the electrolyte and gaseous products.[35]

Durability is another important factor when evaluating electrocatalysts; it was studied by conducting accelerated cyclic voltammetry between potentials of 0.050 V and −0.150 V *vs.* RHE at a scan rate of 50 mV s^{-1} for 1000 potential cycles. That there was no significant reduction in the current densities (Fig. 4e) demonstrated the excellent operational stability of the as-prepared catalyst. Also, we performed chronopotentiometry tests at two different current densities of 30 mA cm^{-2} and 1 A cm^{-2} for over 25 hours (Fig. 4f). No dramatic change in the potential is detected, further confirming the exceptional operational stability of the CoP/Ni_5P_4/CoP catalyst in acid at a very high current density. Additionally, we examined the structure, phase and surface chemical composition of the electrocatalyst after performing a 1000 CV cycle polarization test, *via* SEM,

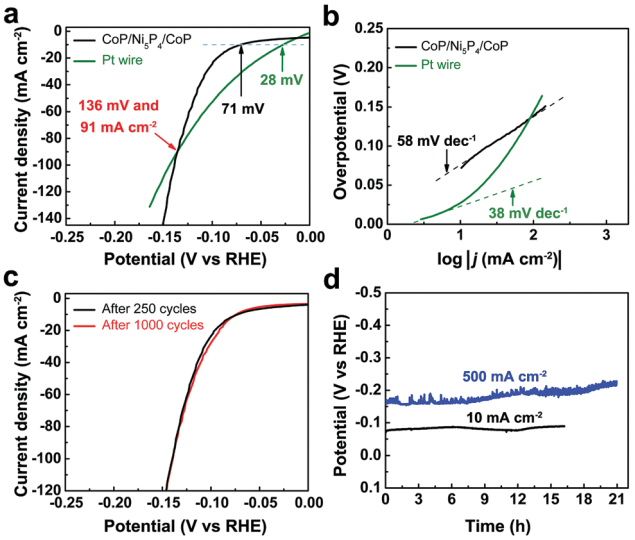

Fig. 5 The electrochemical performance of a CoP/Ni_5P_4/CoP microsheet array electrode in 1.0 M KOH. (a) Polarization curves recorded using CoP/Ni_5P_4/CoP and Pt wire. (b) Tafel plots of the catalysts from (a). (c) Polarization curves of the CoP/Ni_5P_4/CoP electrode after 250 and 1000 cycles. (d) Chronopotentiometry tests at 10 and 500 mA cm^{-2}.

XRD, and XPS (Fig. S20–S22, ESI†). Evidently, almost no obvious changes are found in the SEM images and XRD patterns, meaning that there is no change in the crystal structures and phases of the catalysts during HER testing. XPS spectra of the Co 2p and P 2p core level peaks of the CoP/Ni_5P_4/CoP electrode after electrochemical testing showed almost-diminished peaks from oxides, possibly due to the reduction of surface oxidation during potential cycling.

The CoP/Ni_5P_4/CoP electrocatalyst also demonstrates promising HER activity under alkaline conditions. Fig. 5 shows the HER performance of CoP/Ni_5P_4/CoP in 1.0 M KOH (pH = 14). The hierarchical CoP/Ni_5P_4/CoP requires only 71 and 140 mV of overpotential to obtain current densities of 10 and 100 mA cm^{-2}, respectively, along with showing a Tafel slope of 58 mV dec^{-1}. The catalytic activity of as-prepared CoP/Ni_5P_4/CoP is relatively inferior to that of Pt at a benchmark current density of 10 mA cm^{-2} in alkaline media, however, it compares favorably with recently reported efficient non-noble-metal based HER catalysts, including NiS_2/MoS_2 (204 mV),[36] and the transition metal phosphides (Table S5, ESI†) CoMoP (81 mV),[37] $(Co_{1-x}Fe_x)_2P$ (79 mV),[38] *etc.* We further investigated the electrochemical performance at large current densities (Fig. 5a). Interestingly, the CoP/Ni_5P_4/CoP electrode shows more efficient catalytic activity than Pt wire at current densities higher than 91 mA cm^{-2}, which is very important for large scale hydrogen production *via* water electrolysis.

Although CoP/Ni_5P_4/CoP shows inferior HER performance to some binary metal-based electrocatalysts, including $MoNi_4$ (15 mV at 10 mA cm^{-2})[39] and NiCoP (32 mV at 10 mA cm^{-2}),[40] in alkaline electrolyte, its pH-universal HER activity over a wide pH range is very compelling. In particular, it is noted that metal phosphosulfides are promising electrocatalysts for hydrogen generation from water splitting in acid or base,[15,41] however, the best catalyst still requires an overpotential of 48 mV to reach a benchmark current density 10 mA cm^{-2} in acid,[15] which is not as efficient as ours (33 mV). A recently reported heterogeneous catalyst based on bimetallic phosphide/sulfide has been reported to have great potential as a bifunctional catalyst for overall water splitting in base, but it shows catalytic HER activity inferior to ours.[41] Our catalyst has a much lower Tafel slope, shows a faster increase in geometric current density with overpotential, requires a lower overpotential (71 mV) to reach 10 mA cm^{-2}, and is especially promising for hydrogen generation over a wide pH range. Furthermore, the reasonable operational stability at high current densities in highly alkaline media, as well (Fig. 5d), is another important feature of the as-prepared electrode, which may be of great potential to be implemented as a sustainable pH-universal hydrogen evolving electrode. Finally, the gas products and relevant faradaic efficiency were evaluated in acid and base electrolytes *via* gas chromatography-based techniques[29] (Fig. S23, ESI†). The efficiency, which reflects the conversion of the electrons involved in the catalytic reaction, is determined to be nearly 100%, meaning that nearly all the electrons are utilized for generating H_2 during water electrolysis.

Conclusions

In conclusion, a highly efficient HER electrocatalyst is developed *via* a facile synthetic approach. The as-prepared hierarchical CoP/Ni_5P_4/CoP microsheet array electrode is binder-free, with a self-supported 3D architecture, and can be directly used as a cathode for the HER. The CoP/Ni_5P_4/CoP microsheet array electrode shows Pt-like activity for HER catalysis with reasonable operational stability at high current densities in acidic as well as alkaline electrolytes. The outstanding HER catalytic activity of this electrode is related to the good mechanical and electrical connections between the CoP catalyst and Ni_5P_4 support, numerous active sites, and high intrinsic catalytic activity of the sandwich-like CoP/Ni_5P_4/CoP electrode. We believe that our study will open up a new exciting avenue toward exploring the design of self-supported 3D robust HER catalysts for large-scale hydrogen production *via* water splitting.

Conflicts of interest

There are no conflicts to declare.

Acknowledgements

This project was supported by the US Department of Energy under a grant DE-SC0010831. S. C. is also thankful for the support from TcSUH from the TcSUH Robert A. Welch Professorships in High Temperature Superconducting (HTSg) and Chemical Materials (E-0001). J. B. acknowledges the support from the Robert A. Welch Foundation (E-1728). H. Z. thanks the supports from Hundred Youth Talents Program of Hunan Province and the 'XiaoXiang Scholar' Talents Foundation of Hunan Normal University in China.

References

1 N. Armaroli and V. Balzani, *Angew. Chem., Int. Ed.*, 2007, **46**, 52–66.
2 J. O. M. Bockris, *Int. J. Hydrogen Energy*, 2002, **27**, 731–740.
3 H. Q. Zhou, F. Yu, J. Y. Sun, R. He, S. Chen, C. W. Chu and Z. F. Ren, *Proc. Natl. Acad. Sci. U. S. A.*, 2017, **114**, 5607–5611.
4 I. Roger, M. A. Shipman and M. D. Symes, *Nat. Rev. Chem.*, 2017, **1**, 1–11.
5 R. B. Gordon, M. Bertram and T. E. Graede, *Proc. Natl. Acad. Sci. U. S. A.*, 2006, **103**, 1209–1214.
6 M. S. Faber and S. Jin, *Energy Environ. Sci.*, 2014, **7**, 3519–3542.
7 H. Vrubel, D. Merki and X. L. Hu, *Energy Environ. Sci.*, 2012, **5**, 6136–6144.
8 L. Guo, Z. Yang, K. Marcus, Z. Li, B. Luo, L. Zhou, X. Wang, Y. Du and Y. Yang, *Energy Environ. Sci.*, 2018, **11**, 106–114.
9 D. Kong, H. Wang, Z. Lu and Y. Cui, *J. Am. Chem. Soc.*, 2014, **136**, 4897–4900.
10 E. J. Popczun, J. R. McKone, C. G. Read, A. J. Biacchi, A. M. Wiltrout, N. S. Lewis and R. E. Schaak, *J. Am. Chem. Soc.*, 2013, **135**, 9267–9270.
11 P. Xiao, W. Chen and X. Wang, *Adv. Energy Mater.*, 2015, **5**, 1500985.
12 Y. M. Shi and B. Zhang, *Chem. Soc. Rev.*, 2016, **45**, 1529–1541.
13 X. D. Wang, Y. F. Xu, H. S. Rao, W. J. Xu, H. Y. Chen, W. X. Zhang, D. B. Kuang and C. Y. Su, *Energy Environ. Sci.*, 2016, **9**, 1468–1475.
14 J. Tian, Q. Liu, A. M. Asiri and X. P. Sun, *J. Am. Chem. Soc.*, 2014, **136**, 7587–7590.
15 M. C. Acevedo, M. L. Stone, J. R. Schmidt, J. G. Thomas, Q. Ding, H. C. Chang, M. L. Tsai, J. H. He and S. Jin, *Nat. Mater.*, 2015, **14**, 1245–1251.
16 C. Tang, L. F. Gan, R. Zhang, W. B. Lu, X. Jiang, A. M. Asiri, X. P. Sun, J. Wang and L. Chen, *Nano Lett.*, 2016, **16**, 6617–6621.
17 J. Mahmood, F. Li, S. M. Jung, M. S. Okyay, I. Ahmad, S. J. Kim, N. Park, H. Y. Jeong and J. B. Baek, *Nat. Nanotechnol.*, 2017, **12**, 441–446.
18 Z. Peng, D. Jia, A. M. Al-Enizi, A. A. Elzatahry and G. Zheng, *Adv. Energy Mater.*, 2015, **5**, 1402031.
19 A. Kundu, J. N. Sahu, G. Redzwan and M. A. Hashim, *Int. J. Hydrogen Energy*, 2013, **38**, 1745–1757.
20 I. K. Mishra, H. Q. Zhou, J. Y. Sun, K. Dahal, Z. S. Ren, R. He, S. Chen and Z. F. Ren, *Mater. Today Phys.*, 2018, **4**, 1–6.
21 E. J. Popczun, C. G. Read, C. W. Roske, N. S. Lewis and R. E. Schaak, *Angew. Chem., Int. Ed.*, 2014, **53**, 5427–5430.
22 M. Ledendecker, S. K. Calderón, C. Papp, H. P. Steinrück, M. Antonietti and M. Shalom, *Angew. Chem., Int. Ed.*, 2015, **54**, 12361–12365.
23 Y. Q. Sun, L. F. Hang, Q. Shen, T. Zhang, H. L. Li, X. M. Zhang, X. J. Lyu and Y. Li, *Nanoscale*, 2017, **9**, 16674–16679.
24 A. P. Grosvenor, S. D. Wik, R. G. Cavell and A. Mar, *Inorg. Chem.*, 2005, **44**, 8988–8998.
25 Y. Nicolet, A. L. de Lacey, X. Vernède, V. M. Fernandez, E. C. Hatchikian and J. C. Fontecilla-Camps, *J. Am. Chem. Soc.*, 2001, **123**, 1596–1601.
26 P. Liu and J. A. Rodriguez, *J. Am. Chem. Soc.*, 2005, **127**, 14871–14878.
27 S. Anantharaj, S. R. Ede, K. Karthick, S. Sam Sankar, K. Sangeetha, P. E. Karthik and Subrata Kundu, *Energy Environ. Sci.*, 2018, **11**, 744–771.
28 H. Q. Zhou, F. Yu, J. Y. Sun, H. T. Zhu, I. K. Mishra, S. Chen and Z. F. Ren, *Nano Lett.*, 2016, **16**, 7604–7611.
29 H. Q. Zhou, F. Yu, Y. F. Huang, J. Y. Sun, Z. Zhu, R. J. Nielsen, R. He, J. M. Bao, W. A. Goddard III, S. Chen and Z. F. Ren, *Nat. Commun.*, 2016, **7**, 12765.
30 A. L. Han, H. L. Chen, H. Y. Zhang, Z. J. Sun and P. W. Du, *J. Mater. Chem. A*, 2016, **4**, 10195–10202.
31 Y. Yang, H. L. Fei, G. D. Ruan, C. S. Xiang and J. M. Tour, *Adv. Mater.*, 2014, **26**, 8163–8168.
32 M. Y. Pi, T. L. Wu, D. Zhang, S. J. Chen and S. X. Wang, *Nanoscale*, 2016, **8**, 19779–19786.
33 P. Xiao, M. A. Sk, L. Thia, X. M. Ge, R. J. Lim, J. Y. Wang, K. H. Lim and X. Wang, *Energy Environ. Sci.*, 2014, **7**, 2624–2629.
34 J. Kibsgaard and T. F. Jaramillo, *Angew. Chem., Int. Ed.*, 2014, **53**, 14433–14437.
35 H. W. Liang, X. D. Zhuang, S. Brüller, X. L. Feng and K. Müllen, *Nat. Commun.*, 2014, **5**, 4973.
36 P. Y. Kuang, T. Tong, K. Fan and J. G. Yu, *ACS Catal.*, 2017, **7**, 6179–6187.
37 Y. Y. Ma, C. X. Wu, X. J. Feng, H. Q. Tan, L. K. Yan, Y. Liu, Z. H. Kang, E. B. Wang and Y. G. Li, *Energy Environ. Sci.*, 2017, **10**, 788–798.
38 Y. W. Tan, H. Wang, P. Liu, Y. H. Shen, C. Cheng, A. Hirata, T. Fujita, Z. Tang and M. W. Chen, *Energy Environ. Sci.*, 2016, **9**, 2257–2261.
39 J. Zhang, T. Wang, P. Liu, Z. Q. Liao, S. H. Liu, X. D. Zhuang, M. W. Chen, E. Zschech and X. L. Feng, *Nat. Commun.*, 2017, **8**, 15437.
40 H. F. Liang, A. N. Gandi, D. H. Anjum, X. B. Wang, U. Schwingenschlögl and H. N. Alshareef, *Nano Lett.*, 2016, **16**, 7718–7725.
41 Y. M. Xin, X. Kan, L. Y. Gan and Z. H. Zhang, *ACS Nano*, 2017, **11**, 10303–10312.